

OPEN ACCESS

Use of Ethylene Carbonate Free Ester Solvent Systems with Alternative Lithium Salts for Improved Low-Temperature Performance in NCM622|| Graphite Li-ion Batteries

To cite this article: Nuwanthi D. Rodrigo et al 2022 J. Electrochem. Soc. 169 110504

View the article online for updates and enhancements.

You may also like

- <u>The Effect of Anionic Surfactant and Stripping Voltammetry on the Signal of Ibrutinib at Nano-Level</u>
 Manolya Müjgan Gürbüz, Burcu Doan-Topal, Esen Bellur Atc et al.
- Thermal Management Optimization for Large-Format Lithium-Ion Battery Using Cell Cooling Coefficient Yingchen Xie, Alastair Hales, Ruihe Li et al.
- To the Nature of Surfactant Adsorption onto Metallic Surfaces: Interaction with Metal or Hydrophobic Effect? Adsorption of Hexylamine on Platinum Gennady I. Ostapenko and Nina A. Kalashnikova



244th ECS Meeting

Gothenburg, Sweden • Oct 8 – 12, 2023

Early registration pricing ends September 11

Register and join us in advancing science!



Learn More & Register Now!





Use of Ethylene Carbonate Free Ester Solvent Systems with Alternative Lithium Salts for Improved Low-Temperature Performance in NCM622|| Graphite Li-ion Batteries

Nuwanthi D. Rodrigo, ^{1,*,=} © Chamithri Jayawardana, ^{1,*,=} © Leah Rynearson, ^{1,*} © Enyuan Hu, ² Xiao-Qing Yang, ^{2,**} © and Brett L. Lucht ^{1,**,z} ©

An investigation of alternative lithium salts, lithium tetrafluoroborate (LiBF4), lithium difluoro(oxalato)borate (LiDFOB) and lithium hexafluorophosphate (LiPF6), in novel ester-based (methyl acetate/fluoroethylene carbonate- MA/FEC or methyl propionate/fluoroethylene carbonate- MP/FEC) electrolyte formulations has been conducted in LiNi $_{0.6}$ Co $_{0.2}$ Mn $_{0.2}$ O $_{0.2}$ C (NCM622)/ graphite cells to improve low temperature cycling performance of lithium ion batteries at -20 °C. Improved low temperature performance was observed with all the lithium salts in MA/FEC electrolyte while comparable room temperature (25 °C) capacities were observed with LiPF6 salt only. Detailed ex-situ analysis of surface films generated with LiBF4, LiDFOB and LiPF6 in esterbased electrolytes reveals that the solid electrolyte interphase (SEI) is predominately composed of lithium salt decompaction products and addition of 10% FEC (by volume%) may not be sufficient at forming a protective SEI.

© 2022 The Author(s). Published on behalf of The Electrochemical Society by IOP Publishing Limited. This is an open access article distributed under the terms of the Creative Commons Attribution 4.0 License (CC BY, http://creativecommons.org/licenses/by/4.0/), which permits unrestricted reuse of the work in any medium, provided the original work is properly cited. [DOI: 10.1149/1945-7111/ac940a]

Manuscript submitted August 25, 2022; revised manuscript received September 30, 2022. Published November 3, 2022.

Supplementary material for this article is available online

Among rechargeable battery technologies, Lithium-ion batteries (LIB) remain the primary option for many applications ranging from consumer electronics to electric vehicles (EV). However over the past few years LIB applications have been further expanded to other areas such as grid scale energy storage and aerospace systems.^{1,2} With such diverse areas of applications, LIBs need to be able to successfully perform over a wide range of operating temperatures, particularly at subzero tempertures.³ However, the performance of LIBs at low temperature is still largely limited by (1) reduced Li⁺ transport properties of the bulk electrolyte and (2) high charge transfer polarization from sluggish kinetics at the interphase (slow de-solvation and intercalation of Li+ particularly for graphite electrodes). 4,5 Since electrolyte plays a crucial role in LIB performance at low temperature, optimization of the electrolyte formulation can be used to improve performance. Therefore, electrolyte formulation developments based on (1) lowering the melting point of the bulk electrolyte, and (2) formation of a low impedance interphase are considered to be some of the key design concepts to improve low temperature performance by enhancing the Li⁺ transportation.

Conventional LIB electrolytes contain ethylene carbonate (EC), which has a high dielectric constant, aiding in lithium ion solvation. EC also actively participates in solid electrolyte interphase (SEI) formation on graphite anodes due to the low reduction potential. 6-8 Unfortunately, EC also has a high melting point (36.5 °C), which leads to lower lithium ion conductivity at subzero temperatures making EC containing electrolytes problematic for low temperature applications. There has been significant interest in reducing the amount of EC in the electrolyte by introducing different esters and other low melting point carbonates as co-solvents. 9-11 Esters are particularly attractive solvents for low temperature electrolyte formulations since they have low viscosity, high dielectric constants and low melting points. Previous investigations have reported that low molecular weight esters in carbonate solvent blends can improve the lithium ion conductivity at low temperature. 12,13 In particular, methyl acetate (MA) has been reported to be used as the sole solvent

Equal Contribution.

ZE-mail: blucht@uri.edu

in electrolytes for LIB for fast charging applications at room temperature. ¹⁴ Both fast charging at room temperature, and low temperature operation of a battery have common challenges associated with slow lithium ion transport in the bulk electrolyte, and sluggish charge transfer kinetics at the electrode/electrolyte interfaces.¹⁵ Therefore, developing a high ester concentration electrolyte formulation can be beneficial for low temperature operations. Though low molecular weight esters like MA provide excellent transport properties that are unmatched even by complex ternary or quaternary solvent blends, ester based formulations have a narrow electrochemical window, particularly at the low potential of lithiated graphite. The MA is continuously decomposed which limits the lifetime of the battery. The reductive decomposition is similar to EC but unlike EC the reductive decomposition of the ester solvents does not result in the generation of a protective film on graphite anode allowing graphite to reversibly lithiate and delithiate. Since the stability of the SEI formed on graphite anodes depends upon the structure of the solvents in the electrolyte formulation, EC is frequently considered an important component of the electrolyte.

In order to eliminate EC from the electrolyte, researchers have introduced SEI forming additives to the ester electrolyte systems. ^{16,17} Dahn et al. showed that upon the addition of vinylene carbonate (VC) to ethyl acetate (EA) or methyl propionate (MP) based electrolyte formulations in NMC|| graphite cells delivers similar capacity retention at high temperature and improved rate performance and lower impedance than observed with standard carbonate electrolytes. ¹⁷ Their work showed that ester based solvents can be used without any EC, when enough VC is added to form a stable SEI. Inspiration has been drawn from this work and improved low temperature performance has also been demonstrated with MP, fluoroethylene carbonate (FEC) and LiPF₆ electrolyte formulations. ¹⁸ A direct comparison between MP and MA electrolytes with FEC compared to the current state of the art electrolyte system (1M LiPF₆ in EC: EMC; 3:7) has been conducted.

In addition to the important effects of the solvents and additives, the lithium salt plays a key role in determining the low temperature performance of LIB. The lithium salt in the electrolytes participates in the SEI formation and thus plays an important role in determining the $R_{\rm CT}$. Frequently investigated anions include PF_6^- , BF_4^- , and $BF_2(C_2O_4)^-$ have varying degrees of association strength with the Li⁺ which will influence the viscosity and the conductivity of the electrolyte. This will directly affect the $R_{\rm CT}$ of the cell as the degree

¹Department of Chemistry, University of Rhode Island, Island, Kingston, Rhode Island 02881, United States of America ²Chemistry Division, Brookhaven National Laboratory, Upton, New York 11973, United States of America

^{*}Electrochemical Society Student Member.

^{**}Electrochemical Society Member.

of ${\rm Li}^+$ solvation/de-solvation is a critical part of charge transfer kinetics. ²⁰ Therefore, it is very important to find the right combination of solvents, additives, and salts for improving the low temperature performance. In this manuscript, the effects of replacing ${\rm LiPF}_6$ with alternative Li salts such as lithium tetrafluoroborate (${\rm LiBF}_4$) or lithium difluoro(oxalato)borate (${\rm LiBF}_2(C_2O_4)$, ${\rm LiDFOB}$) in an ester based electrolyte (MA/FEC) and (MP/FEC) systems have been investigated.

Experimental

Single side coated graphite electrodes and LiNi_{0.6}Co_{0.2}Mn_{0.2}O₂ (NCM622) were provided by the Cell Analysis, Modeling and Prototyping (CAMP) facility, Argonne National Laboratory (ANL) with electrode compositions of 91.83% active material (Superior Graphite SLC1520P), 6.38 mg cm⁻² active material loading and 2% conductive carbon, 6% polyvinylidene difluoride (PVdF) binder and 0.17% oxalic acid as an additive for graphite anodes, and 90% active material content, 9.78 mg cm $^{-2}$ active material loading and 5%conductive carbon and 5% polyvinylidene difluoride (PVdF) binder for NCM622 electrodes. Battery grade fluoroethylene carbonate (FEC), lithium hexafluorophosphate (LiPF₆), lithium difluoro(oxalato)borate (LiDFOB) and lithium tetrafluoroborate (LiBF₄) were obtained from BASF (Germany). Battery grade methyl acetate (MA) and methyl propionate (MP) were supplied by Gotion (USA). All the chemical reagents were stored in an Ar filled glove box (M-Braun) with ≤0.1 ppm moisture level and were used without further purification.

CR 2032 type coin cells were assembled with NCM622 (13.7 mm diameter) and graphite (15 mm diameter) electrodes, three separators [one Whatman GF/D glass microfiber (15.6 mm in diameter) between two Celgard 2325 (19 &15 mm in diameter)], and 100 μ l of electrolyte solution in an argon glove box with oxygen and water contents <1 ppm. Three separators are used to minimize the damage to the electrode surface for ex-situ analysis. Both NCM622 and graphite electrodes were dried at 110 °C under vacuum overnight before cell assembly. The electrolytes investigated include 1 M LiPF₆ in ethylene carbonate (EC): ethyl methyl carbonate (EMC) (3:7 vol%) denoted as standard electrolyte (STD) from Gotion Inc. Ester-based electrolytes were prepared with alternative lithium salts; LiPF₆, LiBF₄ and LiDFOB in a mixture of MA, MP and FEC solvent mixture in a Ar filled glovebox. All the electrolytes tested in this study are summarized in Table I.

The NCM622/graphite full cells were galvanostatically cycled at 25 °C for 5 formation cycles between 3–4.2 V at a rate of C/20 for the first cycle, C/10 for the next two cycles and C/5 for an additional two cycles using a high precision battery cycler (Arbin LBT21084). After the formation cycles at 25 °C, cells were transferred to a temperature chamber (Tenny environmental test chamber) at –20 (+/–1) °C for low temperature rate testing and cycling. After a 6 h equilibration period rate testing was conducted at –20 °C for 15 cycles applying varying charge and discharge C-rates of 0.1C/0.1C, 0.2C/0.2C, 0.3C/0.3C, 0.5C/0.5C, and 0.1C/0.1C respectively for three cycles at each rate. After rate testing, the cells were cycled for 50 cycles at a charge rate of 0.2C and discharge rate of 0.3C at –20 °C. Similarly, for the room temperature (RT, 25 °C) cycling another set of cells were transferred to a temperature chamber

Table I. Electrolyte formulations.

Electrolyte ID	Electrolyte formulation
STD	1 M LiPF ₆ in EC: EMC (3:7 vol%)
LiPF ₆ -MA	1 M LiPF ₆ in MA: FEC (90:10 vol%)
LiPF ₆ -MP	1 M LiPF ₆ in MP: FEC (90:10 vol%)
LiBF ₄ -MA	1 M LiBF ₄ in MA: FEC (90:10 vol%)
LiBF ₄ -MP	1 M LiBF ₄ in MA: FEC (90:10 vol%)
LiDFOB-MA	1 M LiDFOB in MA: FEC (90:10 vol%)
LiDFOB-MP	1 M LiDFOB in MP: FEC (90:10 vol%)

(Fisherbrand Isotemp oven) and after formation cycling these cells were cycled for 100 cycles at a rate of 0.5C. At all temperatures, cells were cycled between 3–4.2 V using a constant current-constant voltage (CC–CV) cycling mode with CV step corresponding to 1/20 of the applied current of each C-rate at the top of charge during formation cycles. For remaining cycling protocols (low temperature rate and long-term cycling, and room temperature long term cycling) CV step corresponds to 1 min duration on the top of the charge. The rate was calculated based on the reversible capacity of NCM622 at 0.1C rate which is 180 mAhg⁻¹. Cells were prepared in triplicate for each electrolyte formulation to confirm reproducibility, representative data is provided. Cell to cell variation is less than 3%.

For X-ray photoelectron spectroscopy (XPS), cells were dissembled in an Ar-glove box after formation cycling and long-term cycling (at the end of cycling at $-20\,^{\circ}\text{C}$). Graphite and NCM 622 electrodes were extracted from fully discharged cells and extracted electrodes were rinsed with 3 \times 500 μ l of extra dry dimethyl carbonate (99+%, Acros, DMC) to remove residual electrolyte and dried under vacuum overnight. XPS measurements were acquired with a Thermo K-alpha system using Al K α radiation (hv = 1486.6 eV) under ultra-high vacuum conditions (<1 \times 10–12 atm) with a measured spot size of 400 μ m. Samples were transferred into the XPS chamber with a vacuum transfer vessel to avoid exposure to air. The binding energy was corrected based on the C 1s of C–C at 285.0 eV.

Infra-red with attenuated total reflectance (IR-ATR) spectra of graphite electrodes and NCM 622 electrodes after formation cycles were obtained on a Bruker Tensor 27 spectrometer, using a Pike MIRacle horizontal ATR accessory equipped with a germanium crystal in a nitrogen-filled glovebox. All spectra were collected with 512 scans at a spectral resolution of 4 cm⁻¹. An atmospheric compensation and baseline correction were applied to all spectra.

The morphology of the surface films on graphite electrodes were examined by ex-situ Field-emission scanning electron microscopy (Zeiss Sigma VP) (FE-SEM) at 7.00 kV with a secondary electron detector (SE2). Graphite electrodes extracted from full cells after formation cycles, at the end of 50 cycles at $-20\,^{\circ}\text{C}$, and at the end of 100 cycles at RT were rinsed with DMC and then transferred to the SEM chamber with minimum air exposure. Elemental distribution of the graphite surface films was obtained with Oxford Instruments X-max $50\,\text{mm}^2$ energy dispersive X-ray spectroscopy (EDX) detector.

Results and Discussion

The low temperature rate performance (-20 °C) along with initial formation cycling capacities of NCM622| graphite cells containing alternative lithium salts in MP and MA based electrolytes with 10% FEC are provided in Figs. 1a-1c. As presented in Fig. 1, reversible capacities during formation cycles were slightly lower for all the ester-based electrolyte formulations compared to the cells cycled with STD electrolyte irrespective of the type of the lithium salt used, while the best performance for an ester based formulation was observed with the LiPF₆-MA electrolyte. This can be taken as an indication for the need of further optimization of the ester based electrolyte formulations by introducing SEI forming additives to improve initial capacities. Even with the low initial capacities, significant improvements in rate performance at low temperature were observed for the cells cycled with ester-based formulations compared to the STD electrolyte. The discharge capacities for cells cycled with the STD electrolyte significantly decrease with higher C-rates, delivering 80 mAhg⁻¹ and 50 mAhg⁻¹ at 0.3C and 0.5C, respectively. There is also a clear trend where the cells containing MA as the cosolvent outperform cells containing MP for faster Crates (from 0.2C to 0.5C) irrespective of the lithium salt.

Significant improvements are observed for cells cycled with LiBF₄-MA and LiDFOB-MA electrolyte at C-rates as high as 0.5C, delivering higher discharge capacities of $\sim \! 80 \text{ mAhg}^{-1}$ and $\sim \! 70 \text{ mAhg}^{-1}$, respectively, compared to the STD electrolyte. Overall, the low temperature rate capabilities are greatly improved

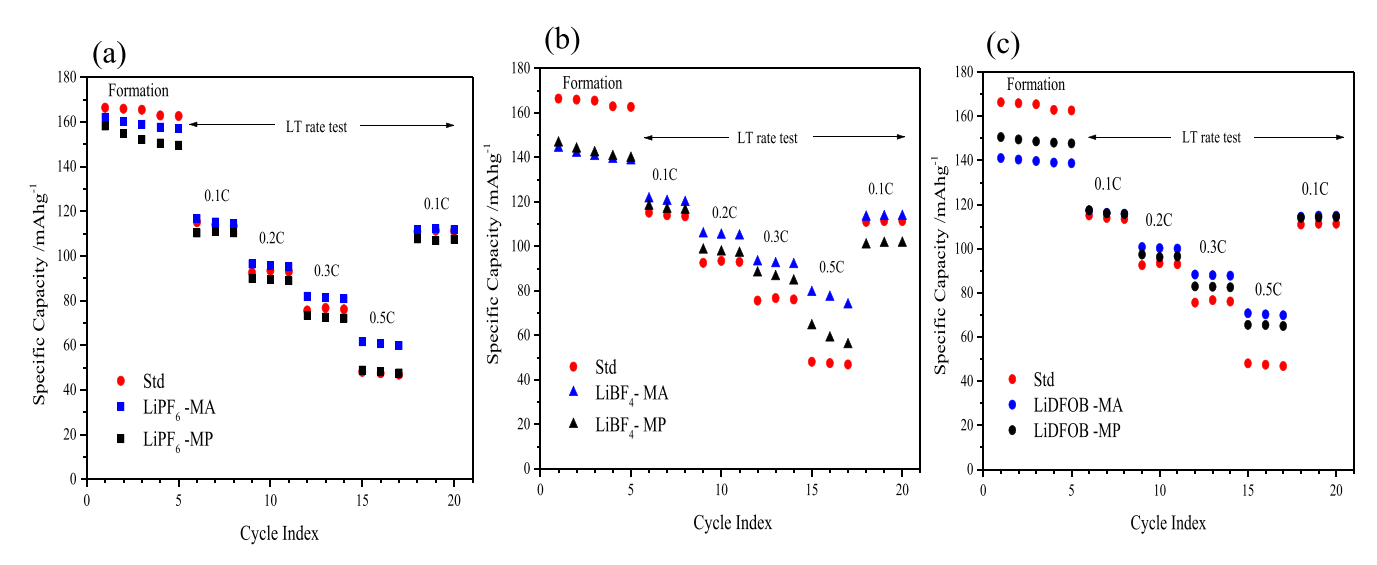


Figure 1. Charge-discharge cycling performance of NMC 622 | graphite cells with (a) 1M LiPF₆ (b) 1M LiBF₄ (c) 1M LiDFOB as the salt at different C rates at −20 °C.

in both MA and MP containing electrolytes in which LiBF4 and LiDFOB have been used as Li salts. The clear trend of improved rate capabilities at low temperature for all ester-based electrolytes regardless of the Li salt is most likely due to the increased conductivity of ester solvent blends (MA or MP/FEC) compared to the analogues carbonate solvent blend (EC/EMC) in the STD electrolyte. 18,21,22 In an interesting, related investigation, the ionic conductivity of a electrolyte system consisting of 1M LiPF₆ in EMC: FEC (19:1) demonstrated relatively a lower conductivity compared to STD. However, in this work we speculate that replacing EMC [melting point: -53 °C, and dielectric constant at 25 °C: 2.985] with lower melting point and high dielectric constant solvent such as MA [melting point: -98 °C, and dielectric constant at 25 °C: 6.68] would likely increase the ionic conductivity of 1M LiPF₆ ester-based electrolyte compared to standard electrolyte. ²³ However, differences in the performance within the ester-based electrolytes arise from the type of lithium salt used and a further study investigating how physical-properties of ester-based electrolytes correlates with improved low temperature performance will be conducted in future. Therefore, a thorough study is needed to understand the interaction of different Li salts anions with solvents and the composition of the interphase at the electrodes.

The comparison of the galvanostatic voltage profiles of NCM622/graphite full cells at their first charge and discharge cycle at different C-rates for ester-based electrolytes with LiPF₆. LiBF₄ and LiDFOB salts at -20 °C is depicted in Figs. 2a–2e. The reduced charge and discharge capacities with increasing C-rate for all the electrolyte formulations is due to the increase in cell polarization during low temperature cycling as depicted in Fig. 2.4 However, cells cycled with LiBF₄-MA and LiDFOB-MA show less polarization than cells with STD electrolyte during charge and discharge at 0.3C and 0.5C which enables cells to deliver more capacity. Interestingly, as depicted in Fig. 2e, cells cycled at -20 °C with LiBF₄-MA electrolyte not only have the lowest polarization but also deliver the highest capacity despite the lower conductivity reported for electrolyte systems containing the LiBF₄ salt.²⁴ The results are consistent with previous investigations that suggest that the lower R_{CT} related to the use of LiBF₄ salt may be the dominant factor for improved low temperature performance. 24,25

Although higher capacity can be obtained with the LiBF₄-MA electrolyte, the presence of a high voltage plateau during 0.5C discharge suggest that lithium plating may be occurring during fast charging at -20 °C. Whereas for the cells cycled with LiDFOB salt in ester-based electrolyte the improved performance may originate from the desirable surface films generated from LiDFOB

decomposition on both the graphite anode and the NMC622 cathode. 27,28

Long term cycling performance at -20 °C for ester-based electrolytes with alternative Li salts are presented in Figs. 3a–3c. Reversible capacities for cells cycled with MA/FEC ester-based electrolyte for all the alternative Li salts outperformed cycling with the STD electrolyte (average capacity of 82 mAhg^{-1}) at the same conditions. While the best capacities were observed for the LiBF₄-MA electrolyte (average capacity of 96 mAhg^{-1}), cells containing the LiDFOB salt in both MA/FEC (average capacity of 94 mAhg^{-1}) and in MP/FEC (average capacity of 87 mAhg^{-1}) have improved low temperature performance. The improved performance observed with MA/FEC is most likely due to the reduced viscosity coming from smaller molecule ester chain of MA compared to MP.

For any potential electrolyte to be used for LIB it is vital for the electrolyte to be able to operate over a wide temperature range. To assess the performance of the ester based alternative Li salt electrolyte formulations long term cycling was conducted in NCM622/graphite cells at RT. As illustrated in Fig. S1, cells cycled with the STD electrolyte have better cycling performance compared to all the ester-based electrolytes irrespective of the type of the Li salt used. However, with all 3 alternative Li salts, the solvent blend with MA/FEC has slightly better performance compared to MP/ FEC. Comparing the different Li salts investigated in both MA and MP ester based electrolytes, LiPF₆ has comparable performance to the STD electrolyte at room temperature. Despite the lower capacity upon cycling at room temperature, both LiDFOB and LiBF₄ salts in MA/FEC have good capacity retention after 100 cycles with a capacity retention of 94% and 84% of their initial RT capacities of 127 mAhg⁻¹ and 105 mAhg⁻¹, respectively. Even though excellent low temperature performance was observed with the alternative Li salts in ester-based solvents, the inferior performance at RT could be due to the instability of the SEI on the graphitic anode. The improved low temperature performance of the ester-based electrolytes is primarily due to the increased electrolyte conductivity from the favorable physicochemical properties of the esters such as low melting points and low viscosities compared to the carbonate counterparts. 18 However, at room temperature, electrolyte conductivity is unlikely to be the most important factor determining the cycling performance. The stability and the composition of the SEI generated on the graphite anode is more likely to be the most important factor in determining capacity retention at RT. In the novel electrolyte systems, the reductive decomposition of FEC may not be sufficient at forming a protective SEI on the graphitic anode which would lead to continuous salt and ester reduction and poor

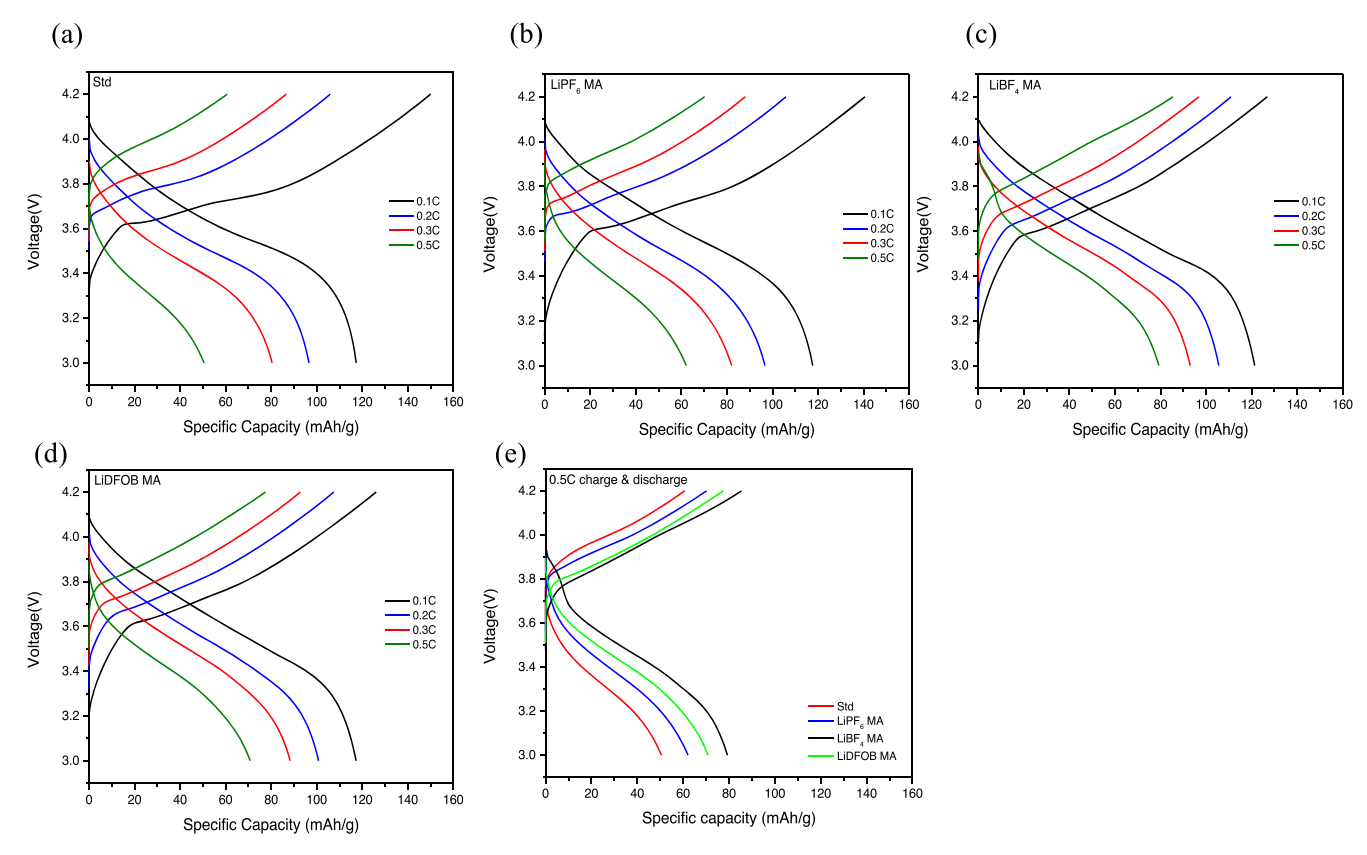


Figure 2. Voltage profiles from the first charge and discharge cycle of NMC 622 | graphite cells with (a) Std (b) 1M LiPF₆ (c) 1M LiBF₄ (d) 1M LiDFOB in MA/FEC based electrolyte at different C rates and (e) first 0.5C charge and first 0.5C discharge voltage profiles for all the salts with MA at -20 °C.

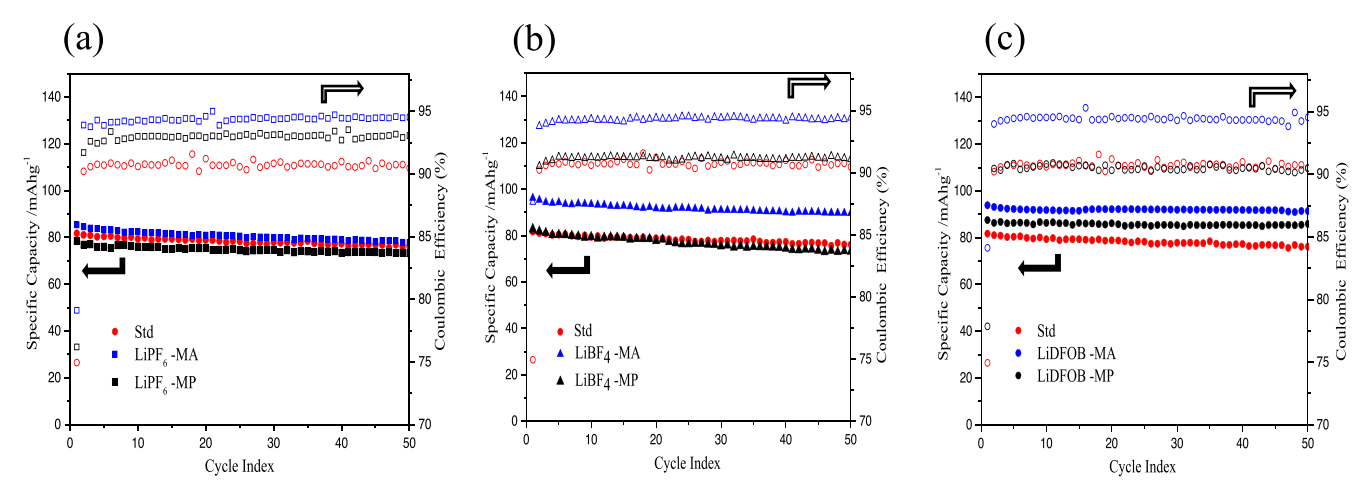


Figure 3. Cycling performance of NMC 622 | graphite cells with (a) 1M LiPF₆ (b) 1M LiBF₄ (c) 1M LiDFOB as the salt at C/5 charge and C/3 discharge rate rates at -20 °C.

cycling performance. The high association strength of LiBF₄ is known for its poor stability at the anode surface. ¹⁹ In the absence of a protective SEI, BF₄ will be continuously reduced at the anode, leading to poorer cycling performance observed during RT cycling. Therefore, further investigations are needed to improve the wide temperature operation of LiBF₄, LiDFOB and LiPF₆ in ester-based systems to uncover a good balance between stable SEI formation and high bulk ionic conductivity.

To understand the composition and the evolution of the surface film formed on the electrodes in the presence of each electrolyte formulation, X-ray photoelectron spectroscopy (XPS) was conducted on the electrodes after formation cycling and after cycling at $-20~^{\circ}\text{C}.^{29}$ C1s, O1s, F1s, B1s and P2p spectra of the surface films

generated on graphite anodes at different stages of cycling with different electrolyte formulations are provided in Fig. 4 and the elemental concentrations of the surface films generated on graphite anodes at different stages of cycling are provided in Table II. Pristine graphite electrodes contain 72% C and 27% F due to the presence of PVdF binder and 1% O from oxalic acid and oxygenated impurities on the surface of the graphite. The relative intensity of the graphite peak at 284.5 eV for C–C/C–H and the total concentration of C are both decreased upon cycling suggesting that the surface of the graphite anodes is covered by a surface film. The initial surface films formed on the graphite electrode differ based on the different Li salt used. The surface film generated on graphite electrodes from the STD electrolyte is composed primarily of organic species including

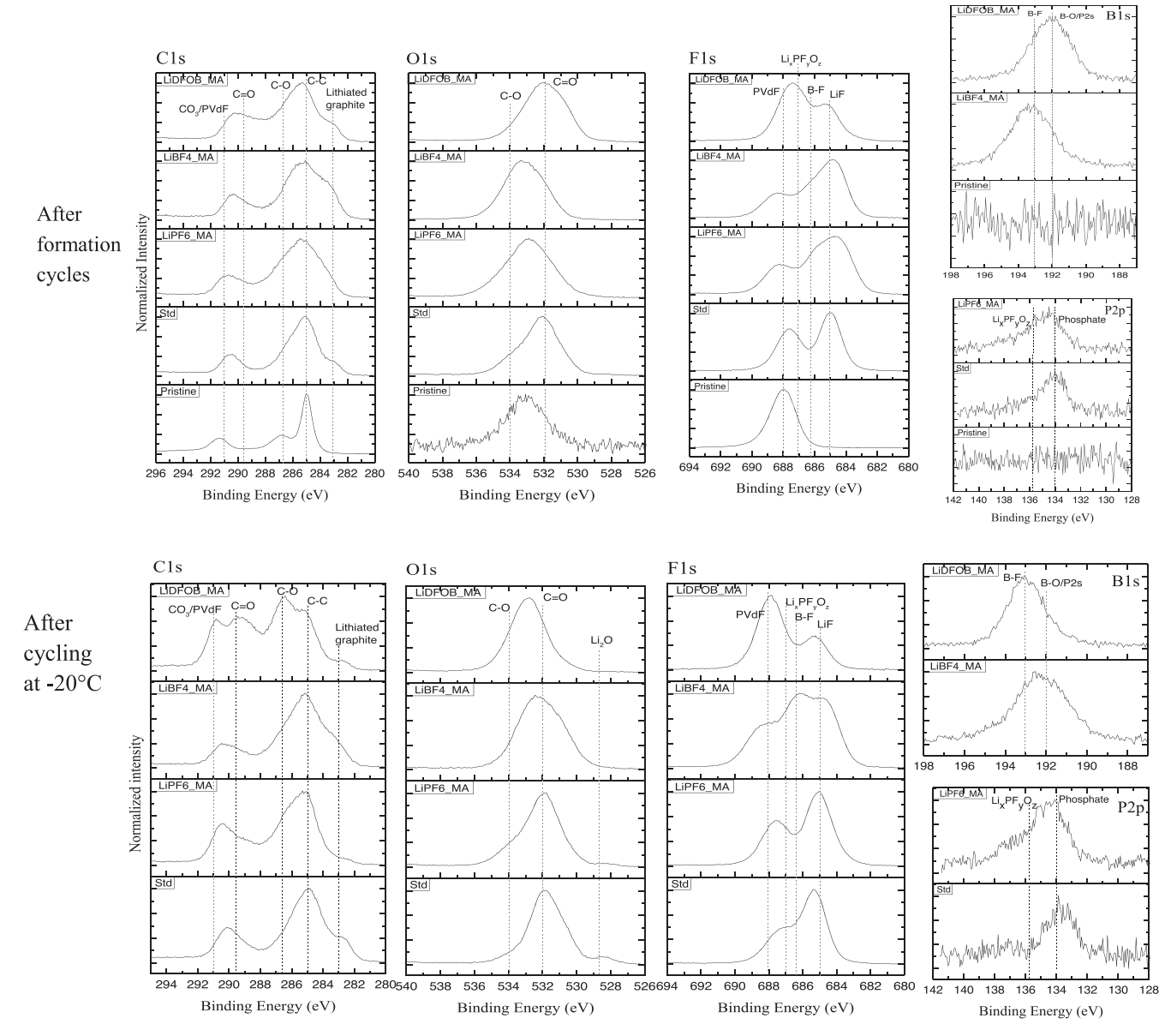


Figure 4. C1s, O1s, F1s, B1s and P2p XPS spectra of the surface films formed on graphite anodes with different electrolyte formulations at different stages of cycling.

Table II. Elemental concentrations of the graphite anode surface films with different electrolyte compositions at different stages of cycling.

	After Formation				After -20 °C Cycling					
	С	О	F	В	P	С	О	F	В	P
Pristine	71.6	1.0	27.4	_	_	71.6	1.0	27.4	_	
Std	38.5	15.8	45.1	_	0.6	38.9	18.8	41.8	_	0.5
LiPF ₆ -MA	39.1	18.6	41.3	_	1.1	37.4	23.6	37.8	_	1.2
LiBF ₄ -MA	26.5	17.9	46.7	8.9		27.5	17.6	46.1	8.8	_
LiDFOB-MA	41.9	27.1	23.9	7.1	_	40.1	32.8	19.9	7.3	_

lithium alkyl carbonates but also contains $\rm Li_2CO_3$ (289 eV and 290.3 eV in C1s) and LiF (685.2 eV in F1s spectra). After formation cycling, cells containing LiBF₄-MA and LiPF₆-MA electrolytes generate a LiF rich initial SEI. This is evidenced by the higher intensity of LiF (685.2 eV) peak compared to the PVdF (688 eV) peak in F1s spectra. In the carbonate based STD electrolyte, the intensity of the LiF (685.2 eV) relative to the

PVdF peak (688 eV) is lower suggesting that the high LiF concentration in LiPF₆-MA electrolyte results from FEC decomposition rather than LiPF₆ decomposition. ¹⁸ The LiBF₄-MA electrolyte formulation has the highest F and B concentrations for the initial SEI, this agrees with the previous reports suggesting that LiBF₄ containing electrolytes generate a LiF, B-O, B-F rich SEI from the BF₄⁻ decomposition. ¹⁹

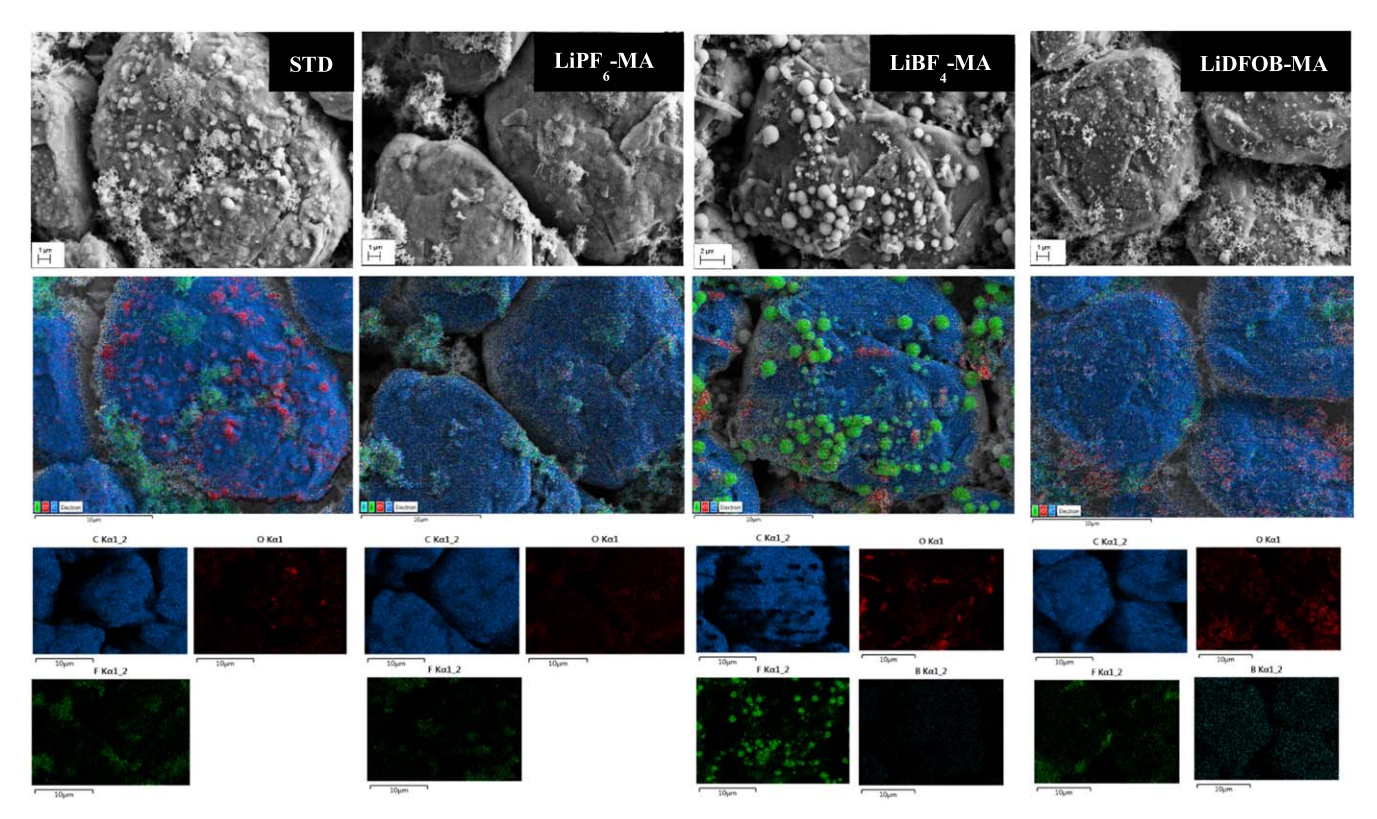


Figure 5. FE-SEM (top) and SEM-EDX overlay images (center) and SEM-EDX elemental mapping (bottom, Blue- Carbon, Red- Oxygen, Green-Fluorine, light blue- Boron) of the SEI layer after 50 cycles at -20 °C with each electrolyte formulation.

The LiDFOB-MA electrolyte generates an SEI with a higher concentration of O than F. This is evident by the much higher O content compared to other electrolyte formulations. The B1s spectrum contains a broad peak corresponding to B-O (192 eV) and B-F (193 eV) species. In the C1s spectra for the LiDFOB-MA electrolyte there is a high intensity peak at 290 eV characteristic of lithium oxalate and other oxalate containing species. ^{19,32,33} The IR-ATR spectra of the graphite anodes after formation cycles (Fig. S2) confirm the generation of the lithium oxalates and other oxalato borate species by the presence of strong peaks at 1760, 1650 and 1320 cm⁻¹ with the LiDFOB-MA electrolyte. ¹⁹ The results support LiDFOB reduction at the anode and formation of an oxalate and oxalato borate rich SEI on the graphite anode.

After cycling at -20 °C for 50 cycles with the STD carbonate electrolyte, more Li₂CO₃, lithium alkyl carbonate (290.3 eV in C1s and 532 eV in O1s spectra) and Li₂O (528.8 eV in O1s) are deposited on the anode surface generating a carbonate rich SEI from solvent decomposition. In cells containing the LiBF₄-MA electrolyte, the intensity of the peak corresponding to the B-F species (686.2 eV in F1s and 193 eV in B1s spectra) has increased along with F and B concentrations on the surface indicating LiBF₄-MA containing cells have a LiF, B-O and B-F rich SEI resulting from the decomposition of BF₄⁻. This agrees with previous investigations which suggest that in the absence of a stable SEI, BF₄ is continuously reductively decomposed. 19 With the LiDFOB-MA electrolyte, prolonged cycling at -20 °C results in a significant increase in O and B containing species (C-O at 286.6 eV, CO₃ at 289 eV, 290.3 eV and poly VC at 291 eV in C1s spectra). The presence of poly(VC) results from the reductive decomposition of FEC. 34,35

FE-SEM images and the SEM-EDX images of the initial SEI formed with each electrolyte formulation are provided in Fig. S3. The SEI generated from the two electrolytes with LiPF₆ have similar morphologies after formation cycles despite the differences in elemental compositions, as observed by XPS spectroscopy. After formation cycling with the LiBF₄-MA electrolyte, spherical LiF

particles are observed on the graphite surface. The spherical particles range in size from about 0.5-1 μ m in diameter and are evenly distributed on the surface. The FE-SEM with EDX layered image and the elemental mapping images of the graphite electrodes after 50 cycles at -20 °C with different electrolyte systems are provided in Fig. 5. After low temperature cycling, SEM images reveal significantly different morphology on the surface of the graphite particles in the two electrolyte systems containing LiPF₆. Graphite particles cycled with the STD electrolyte have a grainy rough surface, the EDX elemental mapping reveals that the granular shaped particles have a high concentration of oxygen. The granular shaped particles are likely EC decomposition species such as Li₂CO₃ and lithium alkyl carbonates.³¹ Graphite anodes cycled with LiPF₆-MA electrolyte generate a much smoother surface film on graphite. The spherical LiF particles formed on the graphite surface in cells containing LiBF₄-MA during the initial formation cycling have not changed in shape or size upon the additional cycling. However, after the long term cycling at -20 °C, rod like structures are observed on the graphite particles which can be identified as plated lithium from the EDX mapping. This confirms that the voltage plateau observed with LiBF₄-MA at high rates in Fig. 2 results from lithium plating. Additional magnifications of FE-SEM images are provided in Fig. S4. Cells cycled at room temperature (25 °C) for 100 cycles with LiBF₄-MA electrolyte also contain spherical LiF particles on graphite electrodes (Fig. S5). The morphology of the graphite surface film generated with LiDFOB-MA electrolyte does not change significantly after 50 cycles at -20 °C.

XPS spectra (O1s, F1s, B1s and P2p) of the surface films formed on NMC622 cathodes after formation cycling and after low temperature cycling with different electrolyte compositions are provided in Fig. S6. Elemental concentrations of the surface films are provided in Table SI. After formation cycling there are only small changes to the surface of the cathode cycled with the STD, LiPF₆-MA and LiBF₄-MA electrolytes suggesting minimal cathode electrolyte interphase (CEI) formation on NCM622 surfaces. This is evident by the presence of the lattice O peak at 529.6 eV in O1s

spectra with these electrolyte formulations. However, considerable changes are observed to the cathode particle surface when the LiDFOB-MA electrolyte is used consistent with the formation of a CEI as evidenced by the disappearance of the lattice O peak and the appearance of B-F and B-O peaks in B1s and F1s spectra. This agrees with the previous reports which indicate LiDFOB generates a passivating film on both the anode and the cathode surfaces. The generation of a passivating film on the cathode likely contributes to the improved LT performance for the LiDFOB-MA formulation. Upon extended cycling at $-20~^{\circ}\text{C}$ there are no significant changes to the CEI formed with the different electrolyte formulations.

Conclusions

In this study, three different lithium salts LiPF₆, LiBF₄ and LiDFOB were investigated in 90% ester (MA or MP) based electrolyte formulations with 10% of FEC over a wide operating temperature range. Compared to the standard carbonate-based electrolyte, cells cycled in MA/FEC electrolyte with all the alternative salts have improved performance at low temperature. Of the three different lithium salts, in MA/FEC ester-based electrolytes formulations, LiBF₄ has the best cycling performance at -20 °C while the LiDFOB salt containing electrolyte has the second best performance having reversible capacities of 96 mAhg⁻¹ and 94 mAhg⁻¹ respectively. However, upon replacing MA by MP, a decrease in reversible capacities is observed which is most likely due to the increased viscosity from replacing the lower molecular weight MA by relatively higher molecular weight MP. In contrast, the initial room temperature capacity is lower for the ester-based electrolytes with LiBF₄ and LiDFOB, while the LiPF₆ salt containing ester electrolytes have comparable initial capacity and capacity retention to the STD electrolyte. Even though excellent low temperature performance was observed with the alternative Li salts in ester-based solvents due to the increased electrolyte conductivity from the favorable physicochemical properties of the esters, the inferior performance at RT is likely due to the instability of the SEI on the graphitic anode. Therefore, electrolyte conductivity is unlikely to be the most important factor determining the cycling performance at room temperature instead the composition and the stability of the anode SEI is the most important factor. Ex-situ surface analysis of graphite anodes cycled with alternative salts in ester-based electrolytes reveals that continuous electrolyte decomposition, particularly decomposition of the salt anion occurs upon long term cycling generating an SEI primarily composed of lithium salt decomposition products. This further suggests that the reductive decomposition of FEC may not be sufficient at forming a protective SEI on the graphitic anode for these ester based electrolyte formulations. Further investigation is needed to successfully employ these novel electrolyte systems over a wide operating temperature range by finding the right balance between stable SEI generation and high bulk ionic conductivity.

Acknowledgments

This work was supported by the Assistant Secretary for Energy Efficiency and Renewable Energy, Vehicle Technology Office of the U.S. DOE through Applied Battery Research for Transportation (ABRT) program under contract No. DE-SC0012704. The electrodes used in this study were produced at the U.S. Department of Energy's (DOE) CAMP (Cell Analysis, Modeling and Prototyping) Facility, Argonne National Laboratory. The CAMP Facility is fully

supported by the DOE Vehicle Technologies Office (VTO). FE-SEM resources were provided by the Rhode Island Consortium for Nanoscience and Nanotechnology, which is supported in part by the National Science Foundation under the Established Program to Stimulate Competitive Research (EPSCoR) Cooperative Agreement OIA-1655221.

ORCID

Nuwanthi D. Rodrigo https://orcid.org/0000-0003-4312-9536 Chamithri Jayawardana https://orcid.org/0000-0002-3144-6377 Leah Rynearson https://orcid.org/0000-0003-3472-7630 Xiao-Qing Yang https://orcid.org/0000-0002-3625-3478 Brett L. Lucht https://orcid.org/0000-0002-4660-0840

References

- 1. B. Scrosati, J. Hassoun, and Y. K. Sun, Energy Environ. Sci., 4, 3287 (2011).
- R. A. Marsh, S. Vukson, S. Surampudi, B. V. Ratnakumar, M. C. Smart, M. Manzo, and P. J. Dalton, *J. Power Sources*, 97–98, 25 (2001).
- 3. J. Hou, M. Yang, D. Wang, and J. Zhang, Adv. Energy Mater., 10, 1904152 (2020).
- 4. S. S. Zhang, K. Xu, and T. R. Jow, J. Power Sources, 115, 137 (2003).
- 5. S. S. Zhang, K. Xu, and T. R. Jow, *Electrochim. Acta*, 48, 241 (2002).
- 6. K. Xu, Chem. Rev., 104, 4303 (2004).
- 7. K. Xu, *Chem. Rev.*, **114**, 11503 (2014).
- D. M. Seo, D. Chalasani, B. S. Parimalam, R. Kadam, M. Nie, and B. L. Lucht, *Electrochem. Lett.*, 3, A91 (2014).
 M. C. Smart, B. L. Lucht, S. Dalavi, F. C. Krause, and B. V. Ratnakumar,
- J. Electrochem. Soc., 159, A739 (2012).
- M. C. Smart, B. V. Ratnakumar, K. B. Chin, and L. D. Whitcanack, *J. Electrochem. Soc.*, 157, A1361 (2010).
- S. I. Tobishima, K. Hayashi, K. I. Saito, and J. I. Yamaki, *Electrochim. Acta*, 40, 537 (1995).
- 12. M. S. Ding and T. R. Jow, J. Electrochem. Soc., 152, A1199 (2005).
- S. Herreyre, O. Huchet, S. Barusseau, F. Perton, J. M. Bodet, and P. Biensan, J. Power Sources, 97–98, 576 (2001).
- X. Ma, R. S. Arumugam, L. Ma, E. Logan, E. Tonita, J. Xia, R. Petibon, S. Kohn, and J. R. Dahn, J. Electrochem. Soc., 164, A3556 (2017).
- E. R. Logan, E. M. Tonita, K. L. Gering, J. Li, X. Ma, L. Y. Beaulieu, and J. R. Dahn, *J. Electrochem. Soc.*, 165, A21 (2018).
- N. D. Rodrigo, C. Jayawardana, and B. L. Lucht, *J. Electrochem. Soc.*, 169, 030519 (2022)
- 17. R. Petibon, J. Harlow, D. B. Le, and J. R. Dahn, *Electrochim, Acta*, **154**, 227 (2015).
- Y. G. Cho, M. Li, J. Holoubek, W. Li, Y. Yin, Y. S. Meng, and Z. Chen, ACS Energy Lett., 6, 2016 (2021).
- 19. M. Nie and B. L. Lucht, *J. Electrochem. Soc.*, **161**, A1001 (2014).
- 20. B. Nan et al., Angew. Chem. Int. Ed., e202205967 (2022).
- E. R. Logan, D. S. Hall, M. M. E. Cormier, T. Taskovic, M. Bauer, I. Hamam, H. Hebecker, L. Molino, and J. R. Dahn, *J. Phy. Chem. C*, 124, 12269 (2020).
- 22. J. Holoubek et al., ACS Energy Lett., 5, 1438 (2020).
- 23. J. Landesfeind and H. A. Gasteiger, J. Electrochem. Soc., 166, A3079 (2019).
- 24. S. S. Zhang, K. Xu, and T. R. Jow, Electrochem. Communications, 4, 928 (2002).
- 25. S. S. Zhang, K. Xu, and T. R. Jow, Electrochemical Acta, 49, 1057 (2004).
- 26. R. V. Bugga and M. C. Smart, *ECS Trans.*, **25**, 241 (2010).
- W. Huang, L. Xing, R. Zhang, X. Wang, and W. Li, J. Power Sources, 293, 71 (2015).
- 28. N. D. Rodrigo, S. Tan, Z. Shadike, E. Hu, X. Q. Yang, and B. L. Lucht, J. Electrochem. Soc., 168, 070527 (2021).
- W. Li, A. Xiao, B. L. Lucht, M. C. Smart, and B. V. Ratnakumar, *J. Electrochem. Soc.*, 155, A648 (2008).
- M. Nie, D. P. Abraham, D. M. Seo, Y. Chen, A. Bose, and B. L. Lucht, *J. Phy. Chem. C*, 117, 25381 (2013).
- 31. S. K. Heiskanen, J. Kim, and B. L. Lucht, *Joule*, **3**, 2322 (2019).
- 32. M. L. Lazar and B. L. Lucht, J. Electrochem. Soc., 162, A928 (2015).
- N. Ehteshami, L. Ibing, L. Stolz, M. Winter, and E. Paillard, J. Power Sources, 451, 227804 (2020).
- A. L. Michan, B. S. Parimalam, M. Leskes, R. N. Kerber, T. Yoon, C. P. Grey, and B. L. Lucht, *Chem. Mater.*, 28, 8149 (2016).
- K. Uta Schwenke, S. Solchenbach, J. Demeaux, B. L. Lucht, and H. A. Gasteiger, J. Electrochem. Soc., 166, A2035 (2019).
- 36. Q. Dong et al., ACS Appl. Energy Mater., **3**, 695 (2020).